10-2004

NOAO Fundamental Plane Survey. I. Survey Design, Redshifts, and Velocity Dispersion Data

Russell J. Smith
University of Waterloo

Michael J. Hudson
University of Waterloo

Jenica E. Nelan
Dartmouth College

Stephen A. W Moore
University of Durham

Stephen J. Quinney
University of Durham

See next page for additional authors

Authors
Russell J. Smith, Michael J. Hudson, Jenica E. Nelan, Stephen A. W Moore, Stephen J. Quinney, Gary A. Wegner, John R. Lucey, Roger L. Davies, Justin J. Malecki, David Schade, and Nicholas B. Suntzeff

The Astronomical Journal, 128:1558–1569, 2004 October

NOAO FUNDAMENTAL PLANE SURVEY. I. SURVEY DESIGN, REDSHIFTS, AND VELOCITY DISPERSION DATA

Russell J. Smith,[1,2] Michael J. Hudson,[1,3] Jenica E. Nelan,[3,4] Stephen A. W. Moore,[3,5] Stephen J. Quinney,[2,3,5] Gary A. Wegner,[3,4] John R. Lucey,[2,3,5] Roger L. Davies,[6] Justin J. Malecki,[1] David Schade,[3,7] and Nicholas B. Suntzeff[8]

Received 2003 November 3; accepted 2004 July 1

ABSTRACT

We introduce the NOAO Fundamental Plane Survey (NFPS), a wide-field imaging/spectroscopic study of rich, low-redshift galaxy clusters. The survey targets X-ray–selected clusters at $0.010 < z < 0.067$, distributed over the whole sky, with imaging and spectroscopic observations obtained for 93 clusters. This data set will be used in investigations of galaxy properties in the cluster environment and of large-scale velocity fields through the fundamental plane. In this paper, we present details of the cluster sample construction and the strategies employed to select early-type galaxy samples for spectroscopy. Details of the spectroscopic observations are reported. From observations of 5479 red galaxies, we present redshift measurements for 5388 objects and internal velocity dispersions for 4131. The velocity dispersions have a median estimated error ~7%. The NFPS has ~15% overlap with previously published velocity dispersion data sets. Comparisons to these external catalogs are presented and indicate typical external errors of ~8%.

Key words: galaxies: clusters: general — galaxies: distances and redshifts — galaxies: elliptical and lenticular, cD — surveys

Online material: machine-readable tables

1. INTRODUCTION

Rich clusters of galaxies have long been recognized as valuable tools with which to study cosmology and galaxy formation. They are the most massive virialized objects in the universe and, as such, provide excellent laboratories for studying the influence of environment on galaxy formation, with the morphology-density relation (Dressler 1980) being a classic example of such an effect. On the cluster outskirts, galaxies are still falling in for the first time, so it is possible to explore environmental effects over a wide dynamic range in density.

Clusters also contain large populations of galaxies at a common distance, which can be used to derive redshift-independent relative distance estimates (e.g., Aaronson et al. 1986; Dressler et al. 1987). This allows the study of deviations from pure Hubble flow, i.e., the peculiar velocity field, and hence the dark matter distribution in the local universe (e.g., Lynden-Bell et al. 1988; see also Dekel 1994; Strauss & Willick 1995 for reviews). Although some recent cluster-based peculiar velocity studies (Lauer & Postman 1994; Hudson et al. 1999, 2004; Dale et al. 1999; Willick 1999; Colless et al. 2001) appear to yield inconsistent results, in fact, when errors arising from sparse sampling of the peculiar velocity field are properly accounted for, there is no significant conflict between these surveys (Hudson 2003). However, the uncertainties in these studies are large, and there remains the possibility of systematic errors due to heterogeneous observing setups.

With these issues in mind, we initiated the NOAO Fundamental Plane Survey (hereafter NFPS), which was supported from 1999 to 2002 under the NOAO Surveys Program. The broad aims of the NFPS are twofold. The first goal is to obtain a precise and definitive measurement of cosmic flows, on scales of $\sim 100\ h^{-1}$ Mpc, using fundamental plane distance estimates for a large, all-sky sample of clusters. The NFPS was designed from the outset to use identical instrumentation to the maximum extent possible in a survey of its kind and to include substantial repeat observations to control for remaining systematics.

The second goal of the NFPS is to obtain a large, homogeneous, and high-quality spectroscopic and imaging data set with which to investigate the interrelationships between morphology, luminosity, and stellar populations, as well as environmental influences on the formation and evolution of early-type galaxies. The NFPS will establish in detail the properties of low-redshift clusters and cluster galaxies and will provide a benchmark for comparison with data at higher redshifts.

The selection of target clusters is driven by these twin objectives. For peculiar velocity studies, it is necessary that the cluster sample have balanced sky coverage in order to avoid degeneracies between the monopole and the dipole of the flow field. Furthermore, because peculiar velocity errors grow linearly with distance, the clusters must be relatively nearby. For the NFPS, we selected clusters with $|b| > 20^\circ$ to a depth of

[1] Department of Physics, University of Waterloo, Waterloo, Ontario N2L 3G1, Canada.
[2] Visiting Astronomer, Cerro Tololo Inter-American Observatory, National Optical Astronomy Observatory, which is operated by the Association of Universities for Research in Astronomy, Inc. (AURA) under cooperative agreement with the National Science Foundation.
[3] Visiting Astronomer, Kitt Peak National Observatory, National Optical Astronomy Observatory, which is operated by the Association of Universities for Research in Astronomy (AURA), Inc.,under cooperative agreement with the National Science Foundation.
[4] Department of Physics and Astronomy, Dartmouth College, 6127 Wilder Laboratory, Hanover, NH.
[5] Department of Physics, University of Durham, Rochester Building Science Laboratories, South Road, Durham DH1 3LE, UK.
[6] Department of Astrophysics, University of Oxford, Denys Wilkinson Building, Keble Road, Oxford OX1 3RH, UK.
[7] National Research Council of Canada, Herzberg Institute of Astrophysics, 5071 West Saanich Road, Victoria, BC V9E 2E7, Canada.
[8] Cerro Tololo Inter-American Observatory, Casilla 603, La Serena, Chile.

$z_{\rm CMB} \sim 0.067$. At these distances, the $\sim 1^\circ$ fields of view of the KPNO and Cerro Tololo Inter-American Observatory (CTIO) Mosaic imagers and of the Hydra spectrographs at WIYN and CTIO allow us to sample clusters out to clustercentric radii of $\sim 1\ h^{-1}$ Mpc. For other purposes, such as the determination of the mass function of clusters, it is necessary to obtain a sample with well-defined selection criteria. We use X-ray luminosity as a proxy for cluster mass, to which it appears to be tightly correlated (e.g., Reiprich & Böhringer 2002). X-ray selection has the further advantage of being less susceptible than the optical galaxy richness to the effects of projection along the line of sight.

The purpose of this paper is to present details of the survey strategy, as well as the primary spectroscopic data. The paper is organized as follows. Details of the cluster selection are given in § 2.1. Within each cluster, we use *B*- and *R*-band photometry to select early-type galaxies for spectroscopic follow-up, as described in §§ 2.2–2.3. In §§ 3.2–3.5 we describe the spectroscopic observations, data reduction, and measurements of redshifts and internal velocity dispersions. Internal and external data comparisons are presented in §§ 3.6–3.7, whereas the process for assigning galaxies to sample clusters is discussed in § 3.8. We conclude with a summary of the data in § 4. Future papers will present additional data, including photometry, morphological parameters, and line strengths, and apply these to studies of cluster distances, galaxy structure, and stellar populations.

2. SURVEY STRATEGY

The overall survey strategy involves six major steps: (1) definition of a cluster target catalog from previous X-ray observations, (2) wide-field imaging observations of the target clusters, (3) color-magnitude selection of early-type galaxy candidates, (4) assignment of spectrograph fibers to targets, (5) spectroscopic observations leading to redshift measurements, and (6) review of the cluster sample in light of improved redshift information.

2.1. *Target Cluster Sample Selection*

The NFPS target clusters are selected from X-ray cluster catalogs derived from the *ROSAT* All-Sky Survey (RASS; Voges 1992). In the northern hemisphere, the target clusters were drawn from the Brightest Cluster Sample (BCS), which is a true X-ray–selected catalog (Ebeling et al. 1998). At the outset of our survey, no similar catalog was available for the southern hemisphere.[9] Our southern targets were therefore drawn from the X-ray brightest Abell clusters (XBACs) sample of Ebeling et al. (1996), providing the X-ray–luminous subset of the optically defined Abell catalog (Abell 1958; Abell et al. 1989). While it is possible that the XBACs may miss massive clusters that were for some reason absent from the Abell catalog, this is less likely to be a problem in the southern hemisphere, since the southern extension by Abell et al. is known to be deeper than the original Abell (1958) catalog (Batuski et al. 1989). Both the BCS and XBACs samples are limited to Galactic latitudes $|b| > 20^\circ$.

The flux limits of the original catalogs are $f_{\rm X} > 4.4 \times 10^{-12}$ ergs cm^{-2} s^{-1} (BCS) and $f_{\rm X} > 5.0 \times 10^{-12}$ ergs cm^{-2} s^{-1} (XBACs). The NFPS clusters were selected from those in the redshift range $0.010 < z_{\rm CMB} < 0.067$, having luminosities $L_{\rm X} > 1.5 \times 10^{43}$ ergs s^{-1} and fluxes $f_{\rm X} > 5 \times 10^{-12}$ ergs cm^{-2} s^{-1}. All X-ray fluxes and luminosities refer to the 0.1–2.4 keV *ROSAT* RASS bandpass. In computing luminosities we assume the cosmological parameters $H_0 = 70$ km s^{-1}, $\Omega_m = 0.3$, and $\Omega_\Lambda = 0.7$.

In order to prioritize the survey observations, we constructed an "A" subsample, designed to be as complete as possible. The A subsample is limited to $z_{\rm CMB} < 0.06$ in order to reduce the number of the most distant clusters, for which morphological analysis requires excellent image quality. The A clusters are further selected by X-ray luminosity, after correcting the fluxes following Hogg & Turner (1998), to reflect the systematic bias affecting low–signal-to-noise ratio (S/N) object detection. This correction depends on the slope of the cluster source-count relation, for which we assume $q = d \log N / d \log S = 1.31$ (Ebeling et al. 1998). We impose luminosity cuts, $L_{{\rm X},c} > 5.0 \times 10^{43}$ ergs s^{-1} for $0.04 < z < 0.06$ and $L_{{\rm X},c} > 2.0 \times 10^{43}$ ergs s^{-1} for $z < 0.04$. The final A subsample is then composed of two overlapping subsets, each volume-limited in X-ray luminosity. Note that these redshift-luminosity limits correspond to a minimum flux of $f_{{\rm X},c} \approx 6 \times 10^{-12}$ ergs cm^{-2} s^{-1}, comfortably above the BCS/XBACs flux limits. Clusters not belonging to the A subsample, but making the original selection cuts, form the "B" subsample. A few clusters that do not meet the overall selection criteria nonetheless have NFPS data; these are retained as a "C" subsample.

The projected cluster centers have been re-examined, using archival *ROSAT* pointed observations (or RASS images in which pointed data are not available) overlaid onto Digitized Sky Survey (DSS) images. Centers were determined based on dominant galaxies, X-ray peaks, or X-ray centroids, and multiple systems were identified where these are unambiguous (see details in § 3.8). In some cases this leads to a substantial change relative to the original catalog coordinates. Likewise, with the NFPS observations in hand, it has been possible to improve the definition of the cluster redshifts. To account for these cases, the selection process was re-applied, leading to some clusters being reclassified relative to the above criteria. In particular, some clusters drop into the C category, being components of multiple systems (A0160A, 0160B, 3526B, 1631B, 1631C, 1736B, 1831A, and 1831B), objects with *cz* revised upward from the original catalogs (A3497, 3104, and 2124), or clusters with zero X-ray flux after the Hogg & Turner (1998) correction (A1631B and A2382).

Table 1 presents the final cluster sample. Figure 1 shows the clusters in the context of the X-ray selection criteria. The sky distribution of the cluster sample is shown in Figure 2. We note that for those analyses requiring a purely X-ray–selected cluster catalog, the appropriate subsample is formed by A clusters in the northern (BCS) region. Of the 33 clusters in this subset, NFPS spectroscopy was obtained for 27 (82% completeness).

2.2. *Imaging Observations*

Imaging data were obtained using wide-field mosaic cameras at the KPNO 0.9 m and Mayall 4 m telescopes, the CTIO Blanco 4 m telescope, and the Canada-France-Hawaii (CFH) 3.6 m telescope. The fields of view range from $36' \times 36'$ to $59' \times 59'$. Queue-mode CFH observations were obtained primarily for the more distant clusters in the sample, for which subarcsecond imaging is essential for morphological analysis. Observations were obtained in the *B* and *R* bands, with typical exposure times of 60 (*R*) and 150 s (*B*) at the 4 m class telescopes and 400 (*R*) and 600 s (*B*) at the KPNO 0.9 m. Two (or three, at CFH) exposures were taken in each band for each

[9] The catalog of de Grandi et al. (1999) covering part of the region became available after our observational campaign was underway.

TABLE 1

THE NFPS CLUSTER SAMPLE

Cluster	R.A. (J2000)	Decl. (J2000)	l	b	Type[a]	cz_{CMB}[b]	ε_{cz}[b]	N_{cz}[b]	$f_{X,c}$[c]	$L_{X,c}$[c]	ABC[d]	X-Ray[e]	N_σ[f]	Source[g]
RXJ0000	00 00 10.6	+08 16 37	101.81	−52.48	...	11512	...	...	4.69	0.16	B	BCS	...	...
A2717.....	00 03 07.7	−35 55 05	356.18	−77.51	...	14660	...	...	8.85	0.49	B	XBA	...	...
A2734.....	00 11 21.6	−28 51 14	30.53	−81.09	DX	18249	78	46	14.46	1.25	B	XBA	43	C
A0075.....	00 39 26.9	+21 15 18	119.20	−41.53	...	18227	...	...	4.91	0.42	B	BCS	...	...
A0076.....	00 40 00.5	+06 49 05	117.86	−55.94	...	11512	...	...	9.64	0.32	A	BCS	...	...

NOTES.—Units of right ascension are hours, minutes, and seconds, and units of declination are degrees, arcminutes, and arcseconds. The coordinates are those of the cluster center, as judged from visual examination of DSS and *ROSAT* data. For convenience we tabulate positions both in equatorial and galactic coordinates. Table 1 is presented in its entirety in the electronic edition of the Astronomical Journal. A portion is shown here for guidance regarding its form and content.

[a] Key to center types: DX = coordinates of a dominant galaxy coincident (or nearly so) with the X-ray peak; GX = coordinates derived from average of several prominent galaxies coincident (or nearly so) with the X-ray peak; XP = coordinates of an X-ray emission peak, without a clear dominant galaxy; XC = coordinates from approximate centroid of large-scale X-ray emission, ignoring local peaks; DG = coordinates from dominant galaxy or galaxies.

[b] Redshifts here are referred to the cosmic microwave background (CMB) frame and expressed as a recession velocity cz in kilometers per second. The cluster redshifts are derived from our own spectroscopic data when possible; otherwise, they are from BCS/XBACs. When our data are used, we give the error, ε_{cz}, and number of galaxy redshifts, N_{cz}.

[c] X-ray fluxes are tabulated in units of 10^{-12} ergs cm^{-2} s^{-1}, whereas luminosities are in 10^{44} ergs s^{-1}. Fluxes and luminosities refer to the 0.1–2.4 keV *ROSAT* RASS bandpass, corrected according to Hogg & Turner (1998; see text).

[d] Selection subsample to which the cluster belongs (see text).

[e] X-ray catalog from which the cluster was selected, i.e., BCS or XBACs.

[f] Number of member galaxies with velocity dispersion measurements reported in this paper.

[g] Source of NFPS spectra: W=WIYN, C=CTIO.

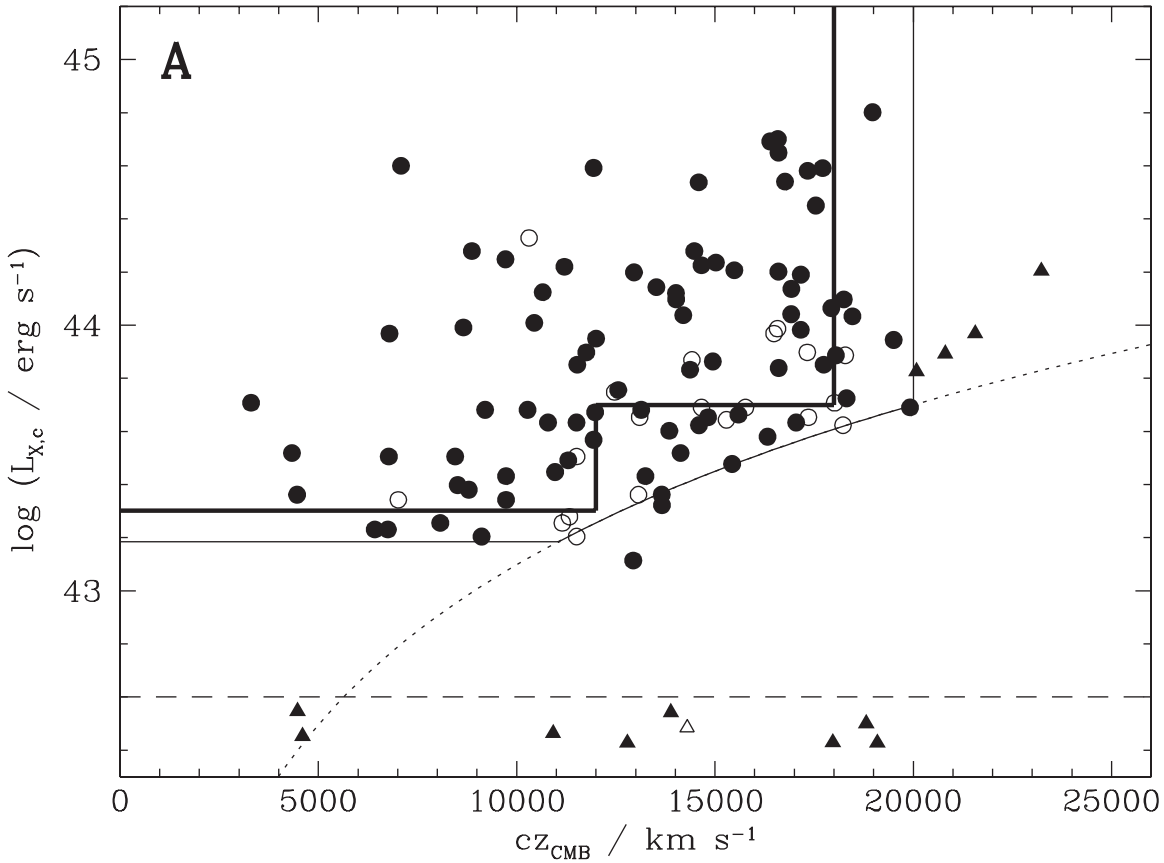

FIG. 1.—X-ray selection of the NFPS cluster sample. The luminosities $L_{X,c}$ are corrected according to the prescription of Hogg & Turner (1998). The thick "stepped" dividing line represents the selection criteria for the A subsample. The thin solid curve shows the B sample selection limits. Clusters without X-ray fluxes are placed below the dashed line, with arbitrary vertical offsets, to show their redshift distribution. A and B sample clusters are represented by circles, whereas C clusters are shown as triangles. Clusters with NFPS spectroscopic data are indicated by filled symbols. Note that a few B objects have fluxes falling below the formal limit (*dotted curve*) after applying the Hogg & Turner correction.

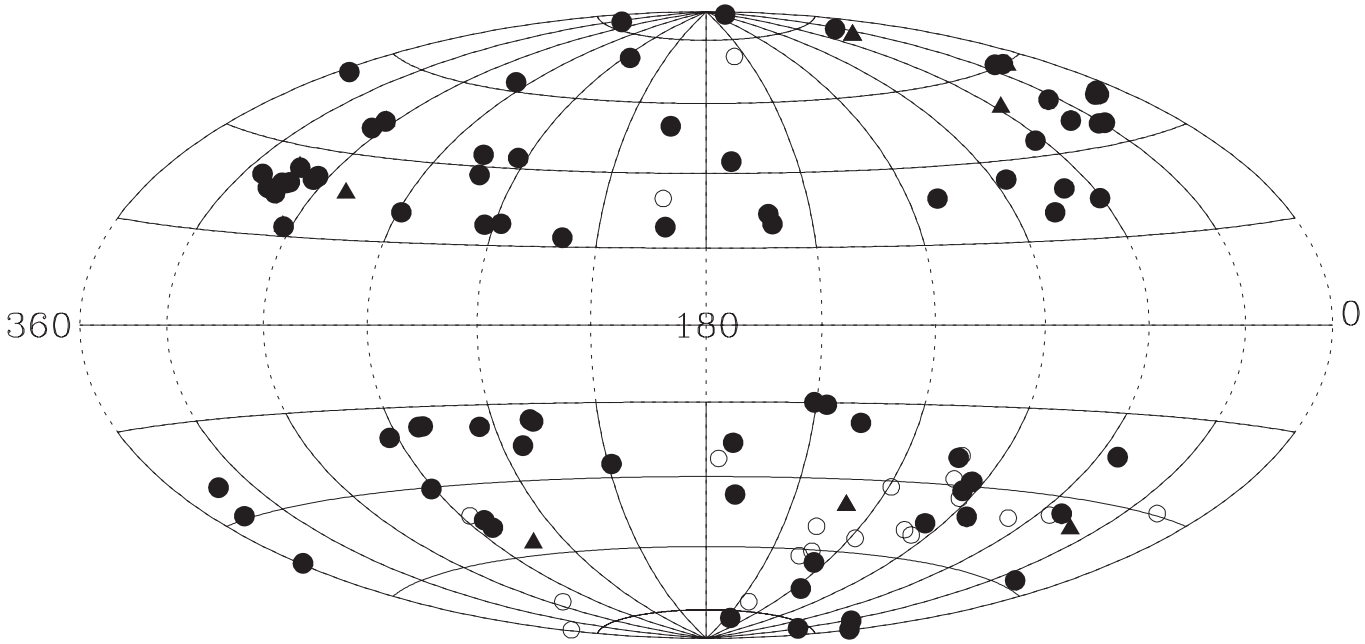

FIG. 2.—Sky distribution of the NFPS sample clusters. The clusters are shown in Galactic coordinates, in Aitoff projection. Symbol types are as in Fig. 1.

cluster, with a small offset to cover most of the area between CCDs in the mosaic. Additional observations were acquired at the MDM 1.3 m telescope, using a single-CCD camera, to provide independent photometric calibration data.

Full details of the imaging data reduction pipeline will be presented in a subsequent paper. The basic reductions were implemented using the *mscred* MOSAIC data reduction package within IRAF. Provisional photometric calibrations, with typical zero-point precision of 0.03 mag, were established using observations of Landolt (1992) and Stetson (2000) standard star fields. (Details of improved calibrations will be reported in a future paper describing NFPS photometry.) However, the absolute calibration is not critical for the purpose of selecting the spectroscopic sample (see below).

For multifiber follow-up, accurate and precise astrometry is a critical requirement. Using the USNO-A2 catalog (Monet et al. 1998) and routines within *mscred*, we were able to achieve precision of $\lesssim 0\farcs1$, as judged from comparisons between overlapping images. This is sufficient to ensure minimal loss of light in the $2''$ diameter fiber apertures of the Hydra instruments.

2.3. *Spectroscopic Sample Selection*

Since it is not practical to observe a complete magnitude-limited sample of member galaxies in each cluster, we are forced to impose some selection criteria to maximize the number of "early-type" targets. Arguably, the optimal selection would be based on morphology alone, e.g., selecting galaxies with a large bulge component after a full two-dimensional decomposition. However, decomposition algorithms are CPU intensive, and effective application of this method would require extensive processing of the input images.

In order to achieve a more rapid turnaround between imaging and spectroscopic observations, we instead applied a galaxy selection method based on the ridge-line populated by early-type galaxies in the $B - R$ color-magnitude diagram. The colors used for this purpose were based on Kron-type total magnitudes from SExtractor (Bertin & Arnouts 1996). These colors are not true matched-aperture colors and so should not be used for more sophisticated analyses. The zero point of the color-magnitude relation was determined empirically, using a median fit to the brighter galaxies (with $R < 16.0$). The slope was assumed uniform for all clusters, in $B - R$ at 0.06 mag mag^{-1} in R. Colors were measured relative to this zero point, making the color selection independent of errors in the provisional photometric calibration, or in the adopted reddenings. The criteria for a galaxy to be targeted for spectroscopic follow-up were then $R < 17.0$ and $\Delta(B - R) > -0.2$. The cut in $\Delta(B - R)$ was established by reference to published morphological types for clusters in common with Dressler (1980). No cut was imposed on the red side of the ridge line, in part to allow for the simultaneous acquisition of a background field galaxy sample. Figure 3 illustrates the color-magnitude selection for two clusters.

Inevitably, color-magnitude selection imposes a bias on the sample observed, since for instance any "blue elliptical galaxies" (i.e., morphologically genuine early types, with colors bluer than normal) would be missed. In the case of cluster A3571, we obtained a repeat observation in which no color cuts were imposed on the galaxy sample. The data for this cluster will be used in future papers, when appropriate, to test the effects of color selection on the wider sample.

3. SPECTROSCOPIC DATA

The spectroscopic observations were obtained in the course of four useful runs (19 nights total, 17 good) at the CTIO Blanco 4 m telescope and seven runs (27 total, 18 good) at the WIYN 3.5 m telescope. The Hydra multifiber spectrographs were used in both cases. The spectroscopic runs are summarized in Table 2.

3.1. *Fiber Assignments*

The color-magnitude selection described above yields target samples ranging from $\sim$50 to $\sim$400 galaxies per cluster. In general, hardware limitations prevent us from obtaining spectra for all of these objects. The principal limitations are

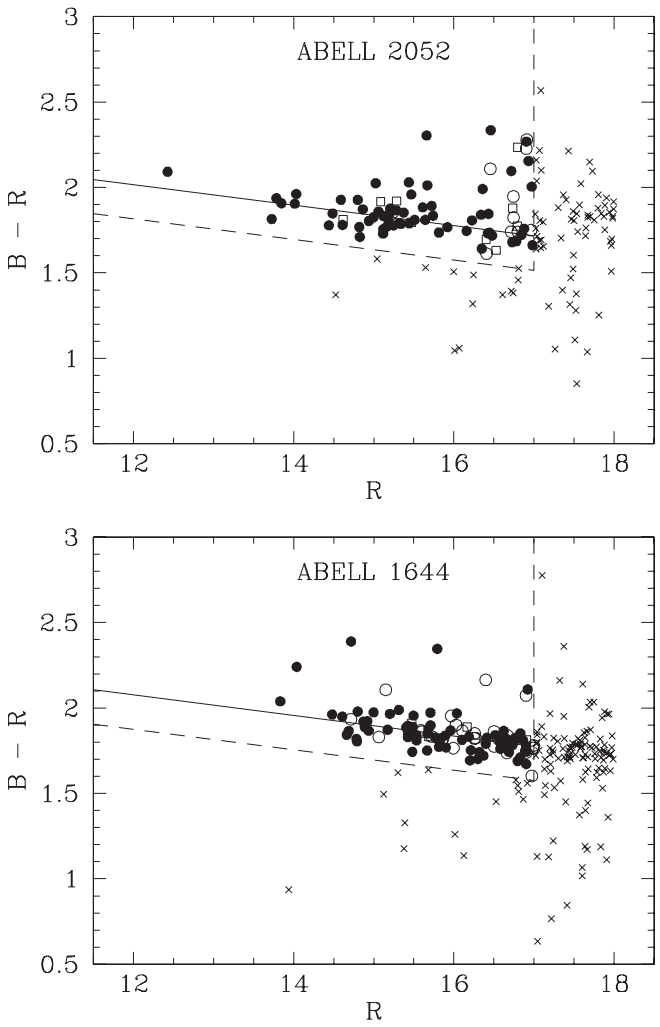

FIG. 3.—Red galaxy selection illustrated for two clusters. The solid line is the color-magnitude relation, with slope 0.06 and zero point fit using a robust scheme. The selection limits in magnitude and color residuals are indicated by dashed lines. Points outside of the selection region are marked as crosses. Inside the selection region, galaxies marked with filled circles were observed with Hydra. Hardware constraints result in some galaxies being unobservable (*open circles*). Open squares mark objects that, although present in the photometric catalog, lie outside the spectroscopic field of view.

the total number of fibers (97 at WIYN, 138 at CTIO), the spectrograph field of view (60′ at WIYN, 40′ at CTIO), the minimum fiber-to-fiber separation on the sky (∼25″), and the maximum angle that the fibers can be bent from a radius on the focal plane (∼5°). Further constraints arise from the need to place a minimum of two bright guide stars in the field of view; in the case of clusters in the Galactic caps, a significant pointing offset is sometimes required to obtain these stars.

The fiber-assignment procedure employed is based on an algorithm by P. Massey (Lowell Observatory). The input catalog is prioritized according to *R*-band magnitude, such that bright galaxies are observed in preference to faint objects. The algorithm is tested over a grid of pointing positions to select the position yielding the most galaxies subject to the guide-star constraint. Often it was possible to assign fibers to a few extra galaxies by manually tweaking the configurations.

A consequence of the fiber-assignment scheme is that the selection function of the observed sample generally has a soft cutoff, with an effective magnitude limit brighter than the original $R < 17$ cut. The selection functions will be fully quantified in a later paper, when the final calibrated photometric catalogs are available.

TABLE 2
NFPS SPECTROSCOPIC OBSERVING RUNS

Run Code	Dates	$D_{\rm fov}$ (arcmin)	$N_{\rm fibers}$	λ Range (Å)
CTIO1[a]	2000 Oct 28–30	40	69	3950–7050
CTIO2	2001 Feb 15–17	40	138	3900–6100
CTIO3	2001 Jun 25–27	40	138	3900–6100
CTIO4	2001 Oct 10–14	40	138	3900–6100
CTIO5	2002 Mar 14–22	40	138	3900–6100
WIYN1	2000 Oct 28–31	60	97	4000–6500
WIYN2	2001 Feb 14–16	60	97	4000–6500
WIYN3	2001 Apr 30–May 01	60	97	4000–6500
WIYN4	2001 May 30–Jun 01	60	97	4000–6500
WIYN5	2001 Oct 08–Oct 14	60	97	4000–6500
WIYN6	2002 Apr 12–14	60	97	4000–6500
WIYN7	2002 May 04–07	60	97	4000–6500

[a] The CTIO1 run used a different camera from runs 2–5. This configuration restricted the instrument to only half the total number of fibers. All CTIO1 observations were later repeated with the full instrumentation; the CTIO1 data are therefore not used in this study and are recorded here for completeness only.

3.2. *Observations*

At CTIO (runs 2–5), the 400 mm Bench Schmidt camera was used with the 632 line mm^{-1} KPGL1 grating, yielding recorded spectra with resolution of 3 Å (FWHM), sampled at 1.15 Å pixel^{-1}. The data cover approximately the range 3900–6100 Å. At WIYN, the "red" fibers and "Bench red" camera were used. The 600 line mm^{-1} grating delivers a resolution of 2.8 Å, sampled at 1.4 Å pixel^{-1}. The spectral range of the WIYN data is 4000–6800 Å. Toward the blue end of the range, the WIYN sensitivity is substantially poorer than that of the CTIO data. In both spectrographs, the projected fiber diameter is 2″.

The integration times were generally 1.5–2.0 hr per observation, broken into three or four individual exposures for cosmic-ray rejection.

3.3. *Data Reduction*

Spectroscopic data reduction was undertaken using standard and custom tasks within IRAF. Variance-weighted extraction was employed as implemented in the *dohydra* task, in conjunction with cleaning of bad pixels and cosmic-ray hits. The spectra were wavelength calibrated using a polynomial fit to 30–50 lines in standard arc lamp spectra. These fits yield typical rms scatter of ∼0.05 Å.

A "master" sky spectrum was derived for each exposure by combining the spectra from 10–30 individual sky fibers. The fibers do not all have identical throughput, and in some runs the differences could not be adequately determined from the calibration "flat-field" spectra obtained. In order to perform accurate sky subtraction, it was therefore necessary to scale the master sky spectrum based on the flux in the bright 5577 Å line to minimize residuals in each galaxy spectrum in turn.

The multiple exposures in each pointing were combined, with rejection of remaining cosmic rays. Error spectra were retained and processed along with the spectra themselves. The error spectra incorporate the noise in the extraction, as well as pixel-by-pixel errors in sky subtraction.

Spectrophotometric standard stars were observed, but in some runs the continuum shape for these spectra differ

markedly from fiber to fiber. Since the galaxy spectra show much smaller fiber-to-fiber variations, we are confident that this does not reflect real differences in the fiber transmissions. Instead of these stars, we therefore use an elliptical galaxy model spectrum from Kinney et al. (1996) as our "flux standard." For ~15 normal early-type spectra in each run, we derive the flux correction curve after redshifting the model to match the observed galaxy, finally averaging these curves to obtain a single global flux correction for each run. The flux calibration thus does not account for fiber-to-fiber transmission differences, but these appear to be small in most cases. Note that although this method of flux calibration forces the average bright galaxy in our survey to have a given spectral shape, the intrinsic galaxy-to-galaxy variations are fully preserved.

As a simple characterization of the data quality, we compute the S/N per angstrom over the range 5000–5500 Å (observed frame). For 6886 spectra obtained, the median S/N is 25 $Å^{-1}$ in both the WIYN and CTIO subsets (Fig. 4).

3.4. *Velocity Dispersion Measurements*

Velocity dispersions and radial velocities were measured using procedures based on the Fourier cross-correlation method (Tonry & Davis 1981), as implemented in the *fxcor* task of IRAF. Briefly, the method computes the cross-correlation of the galaxy spectrum with a template K giant star. The location of the peak yields the redshift, whereas its full width at half-maximum, *W*, can be related to the internal velocity dispersion σ after calibration against broadened-star models.

Depending on the observing run, between 3 and 12 template stars with spectral types G8 to K3 were employed in the *fxcor* measurements. Redshifts were obtained using the full spectral range of the data and referred to the heliocentric frame using template radial velocities obtained from SIMBAD. After measuring the redshift, the spectra were clipped to a common rest-frame spectral range of 4650–5650 Å, before rerunning *fxcor* for the velocity dispersion measurements. A separate *W*-to-σ calibration curve was constructed for each template star, with the velocity dispersions from all adequate *fxcor* runs averaged to produce the final measurements. Fourier filtering is imposed to suppress continuum trends and high-frequency noise, both in the measurement of σ and in establishing the calibration curves. To the extent that the galaxies and stars have similar continua, the effects of filtering cancel in the final σ measurement. To improve the reliability of the measurements, sky-subtraction residuals at 5577 Å were interpolated where necessary, using an automated clipping algorithm that preserves data when possible.

As a consistency test, for one observing run (CTIO3), all σ measurements were repeated using an independent code employing the Fourier quotient (FQ) technique. The FQ code was developed by one of us (J. R. L.) and has been used in many previous fundamental plane studies (e.g., Lucey et al. 1997; Smith et al. 1997, 2000). Comparison of *fxcor* with FQ results for identical input data yields an offset of ~1.5% in σ between the two methods (with FQ measurements being larger) for ~400 galaxies with S/N > 20. The scatter in $\log(\sigma_{\rm FXCOR}/\sigma_{\rm FQ})$ is 0.027, or ~6%. This scatter likely reflects the different ways in which the two algorithms are affected by noise, template mismatch, and non-Gaussian velocity distributions.

3.5. *Robust Redshifts*

The redshifts obtained via *fxcor* are unreliable in cases in which the observed spectrum departs markedly from that of the K giant template, for example, in which the target galaxy exhibits strong emission lines. To determine redshifts with greater robustness, a second set of *fxcor* measurements was made, with a range of templates constructed from "prototypical" observed spectra. The templates include pure absorption and emission-dominated spectra, as well as intermediate types and "poststarburst" (k+a) spectra. For galaxies in which the "best-match" template was *not* a pure absorption spectrum or in which the "robust" redshift deviated by more than ~500 km s^{-1} from the original K giant template redshift, the spectra were inspected by eye to verify the redshift measurement. Additionally, *all* spectra with S/N < 15 $Å^{-1}$ and/or Tonry & Davis (1981) *R*-values less than 3.5 were visually inspected. Generally, the K giant templates yield more precise measurements (due to their smaller intrinsic dispersion) than the templates used for robust measurements. Thus, where the original and robust measurements yield consistent results, the original *cz* values are retained. For 92 low-S/N spectra, no reliable redshift could be determined from this combination of automatic methods and visual inspection.

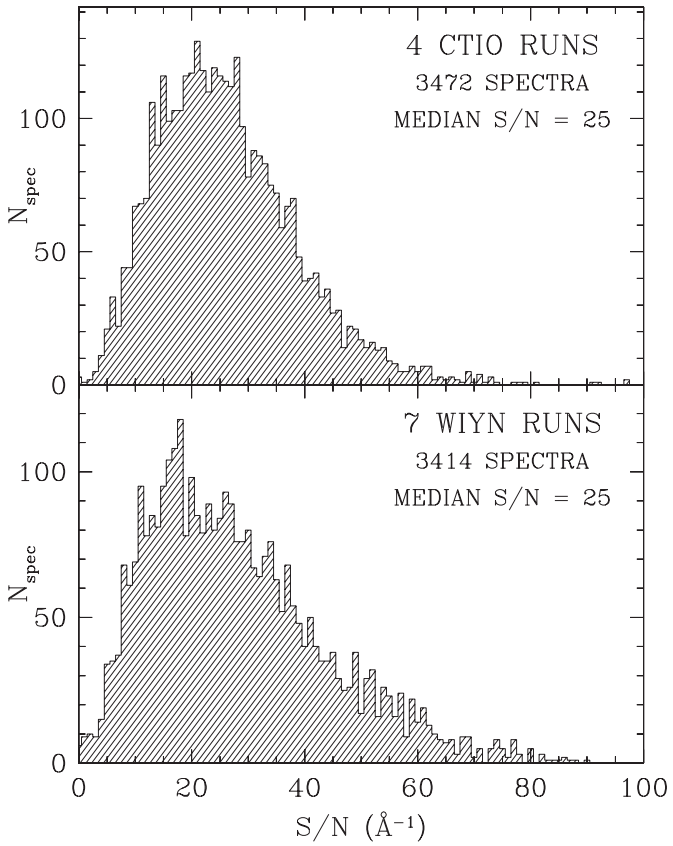

FIG. 4.—Histograms of S/N per angstrom for the individual spectra. Only spectra with S/N > 15 contribute to the velocity dispersion measurements.

3.6. *Comparisons, Errors, and Data Combination*

Substantial telescope time was invested in observing some clusters in two or more observing runs to provide the essential constraints on systematic errors in velocity dispersion. In particular, at least two such "overlap" clusters were observed on every run, so that all runs are well linked to the others. Since some galaxies were observed three or four times, a simultaneous comparison method must be employed to derive consistent offsets between the runs. Here we use an improved version of the method introduced in Smith et al. (1997) and

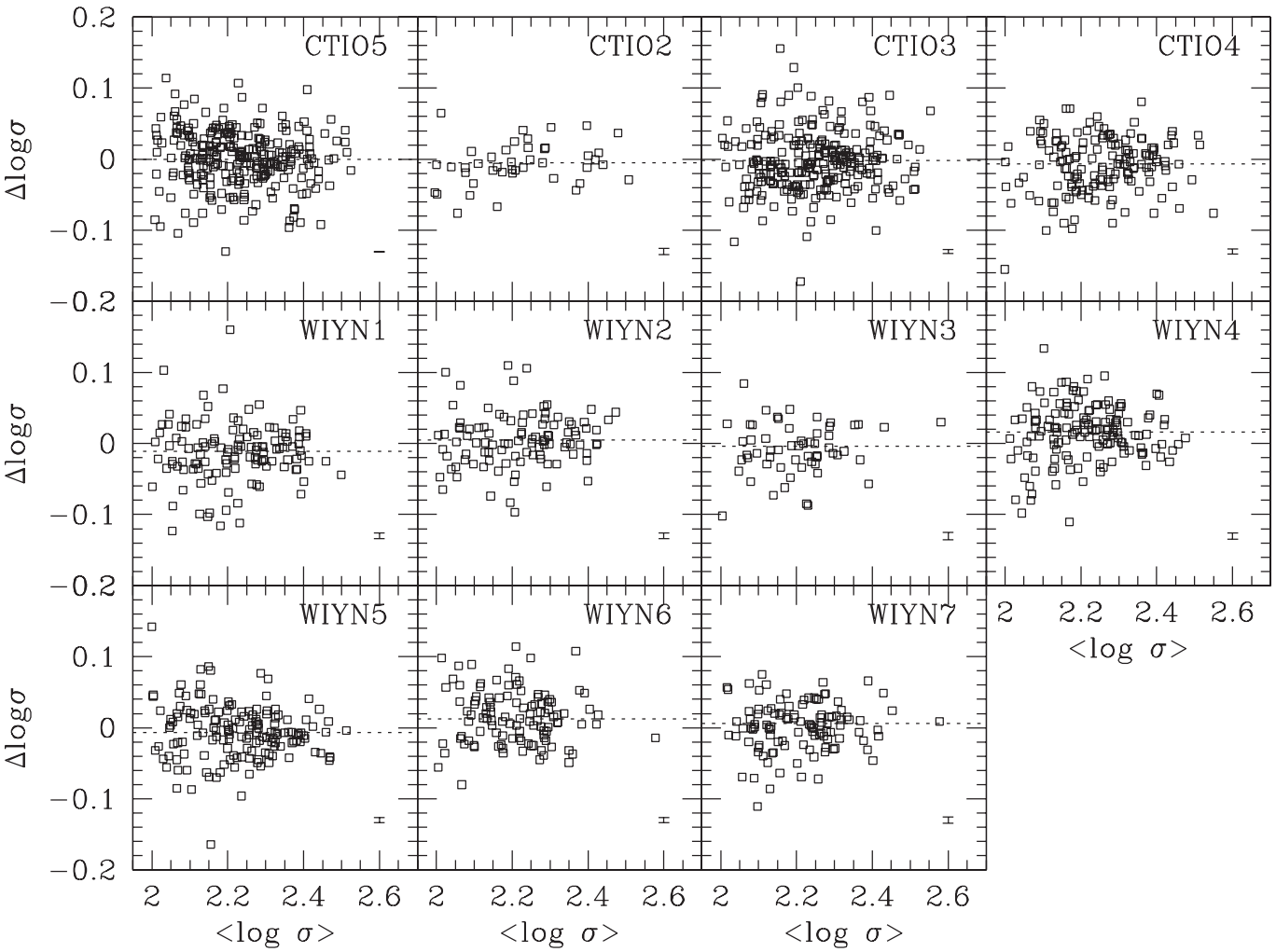

FIG. 5.—Comparisons of repeat measurements of velocity dispersion, σ. For example, in the panel showing run WIYN6, we calculate the average σ of all measurements of all the other runs after corrections and compare the uncorrected WIYN6 values to this average. Thus, the positive offset of WIYN6 from the zero line indicates that this system yields σ values systematically larger than the "base" system and so requires a negative correction. The small error bar at the lower right of each panel indicates the uncertainty in the derived correction.

subsequently used by Wegner et al. (1999) and Hudson et al. (2001).

The overlap sample consists of 1539 measurements for 682 distinct galaxies. While the Hudson et al. analysis assumed all observations had a common error, in this application we allow the errors to vary as a function of S/N, with $\varepsilon_{\log\sigma} = E/(\mathrm{S/N})$. The constant of proportionality here is varied manually; we find that setting $E = 0.9$ yields an acceptable χ^2, given the degrees of freedom. As well as using these errors in determining the run-to-run offsets, we propagate the $\varepsilon_{\log\sigma}$ values into the final catalog to serve as estimates of the random error in each velocity dispersion measurement. As in Hudson et al., the comparisons exclude velocity dispersion measurements below 100 km s^{-1} and those discrepant from the fits by more than 3 σ (the latter representing only $\sim$1% of the total).

The intercomparisons are presented graphically in Figure 5; the offsets derived from the comparisons are recorded in Table 3, together with their errors. Although the CTIO runs yield nearly consistent measurements, the WIYN data exhibit more significant run-to-run shifts. However, we find that overall, the offsets can be determined with errors at the $\sim$0.004 dex level, equivalent to systematic errors of $\lesssim$1.5% in fundamental plane distance. For comparison, the typical system-matching

TABLE 3
CORRECTIONS FOR SYSTEMATIC OFFSETS IN $\log\sigma$

Data Source	N_{comp}	Correction to $\log\sigma$
CTIO2	44	$+0.0053 \pm 0.0045$
CTIO3	249	$+0.0015 \pm 0.0028$
CTIO4	154	$+0.0071 \pm 0.0038$
CTIO5[a]	273	0.0000
WIYN1	123	$+0.0117 \pm 0.0042$
WIYN2	101	-0.0042 ± 0.0037
WIYN3	63	$+0.0051 \pm 0.0050$
WIYN4	149	-0.0163 ± 0.0044
WIYN5	155	$+0.0050 \pm 0.0039$
WIYN6	115	-0.0126 ± 0.0039
WIYN7	113	-0.0063 ± 0.0043

NOTES.—The tabulated quantity is the correction to be added to the raw $\log\sigma$ values to bring all runs onto a common system. The value N_{comp} is the number of galaxies used to derive the correction, after removing low-σ and highly discrepant galaxies.

[a] The base system CTIO5 has zero correction and error, by definition.

error in the Streaming Motion of Abell Clusters (SMAC) compilation was ~0.007 dex (Hudson et al. 1999). A crucial feature of our intercomparison scheme is that the full covariance matrix is derived. For instance, we find that the WIYN1 and WIYN5 data sets, obtained at a similar time of year, are strongly linked to each other so that their offsets tend to move together in the fits. Ultimately, this method can be used to generate mock catalogs of peculiar velocity measurements, properly incorporating the correlation structure of the systematic errors.

The data for cz and $\log \sigma$ are combined using variance-weighted means of multiple observations, and the errors are propagated accordingly. In the case of redshifts, for which an external credibility check has been applied, all measurements are used in the average. For the velocity dispersions, only spectra with $S/N > 15$ Å^{-1} are allowed to contribute to the merged data. The median estimated error in the merged velocity dispersions is 7%.

3.7. *External Comparisons*

Previous spectroscopic surveys have yielded velocity dispersion measurements for approximately 15% of the NFPS sample galaxies, which we employ here to test the reliability of the new data. By far the largest overlap samples are (1) the SMAC catalog of Hudson et al. (2001), with 286 galaxies in common; (2) the Sloan Digital Sky Survey (SDSS) second data release (DR2; Abazajian et al. 2004), with 203 objects in common; and (3) the EFAR catalog (Wegner et al. 1999), with 124 common galaxies. The SMAC and EFAR data sets are merged catalogs, each derived from observations at many different telescopes, while the SDSS sample is arguably of much greater uniformity. Other large velocity dispersion data sets either were subsumed into the SMAC catalog and hence are not independent (e.g., Jørgensen et al. 1995) or have much smaller overlap with NFPS (e.g., the ENEAR sample of Wegner et al. 2003, with only 23 galaxies in common).

For the comparisons, we apply an aperture correction $0.04 \log (r_{\rm ap}/r_{\rm norm})$, normalized to the standard physical aperture size of 1.19 h^{-1} kpc radius (Jørgensen et al. 1995). This reproduces the corrections used by EFAR and SMAC but is not identical to the SDSS correction, which is normalized relative to the effective radius R_e (Bernardi et al. 2003). In the case of the SMAC comparison, we exclude two galaxies with highly discrepant redshift measurements, SMAC identifications A4038:D-054 and A3558:FCP-33. In each case, the NFPS value is confirmed by previous published values (Collins et al. 1995; Teague et al. 1990), suggesting that these are misidentifications in SMAC.

Figures 6*a*–6*c* show the individual NFPS measurements compared to the external data sources as a function of (our) S/N. Some galaxies therefore contribute multiple points to these panels. Recall that spectra with $S/N < 15$ Å^{-1} are not used in deriving the final merged data; they are shown here to illustrate the rapid deterioration in reproducibility at low S/N.

Figures 6*d*–6*f* show the comparisons for the *merged* NFPS velocity dispersion data set, which are further quantified in Table 4. The overall offset of NFPS relative to SMAC and EFAR is ~3%, with NFPS dispersions being smaller. Relative to SDSS, the mean offset is larger (~6%), with a suggestion of a trend that low-σ galaxies have progressively larger offsets. (This trend operates in the sense expected from the R_e-σ relation, combined with the R_e-based aperture normalization applied by SDSS.) The EFAR comparisons show a trend in the opposite sense, possibly dominated by a few points at the extremes of the σ range. For robustness against outliers, we compute a nonparametric scatter, defined as half the range enclosing 68.3% of the points (equivalent to the standard deviation if the differences follow a Gaussian distribution). The scatters are 10.6%, 14.3%, and 12.0% in velocity dispersion for the comparisons to SMAC, SDSS, and EFAR, respectively. It is important to note that the overlap data sets cover different parameter ranges. For instance, the EFAR comparison is dominated by giant galaxies with $\sigma > 150$ km s^{-1}, whereas smaller objects contribute many more points to the overlap with SDSS. From the ~0.05 dex scatter in NFPS−SMAC or NFPS−EFAR, assuming equal contributions from NFPS and SMAC/EFAR, we estimate a characteristic external error of ~8% in the velocity dispersions.

In Figures 6*g*–6*i* we show the equivalent comparisons for redshift measurements. The median offsets are −7, +11, and +13 km s^{-1}, compared to SMAC, SDSS, and EFAR, respectively, with a scatter of ~30 km s^{-1} in each case. These comparisons are limited to galaxies that have velocity dispersion measurements, and therefore the comparison redshifts are generally based on spectra of high quality. Naturally, however, redshifts have been published for many more of the galaxies, from studies of individual clusters or in wide-angle redshift surveys. Searching the NASA Extragalactic Database (NED), we find redshift data for 3004 (~55% of the NFPS sample), from which we obtain a median offset of NFPS − NED = $+6 \pm 2$ km s^{-1}. The data quality and positional accuracy in NED vary widely, causing a handful of highly discrepant points. The nonparametric scatter estimate is ~70 km s^{-1}.

3.8. *Cluster Assignments*

The assignment of galaxies to individual clusters is inevitably a subjective exercise; in the case of clusters that overlap in redshift and projected location, it is not clear that any assignment scheme will be meaningful. Moreover, assignments appropriate for one application of the data may not be optimal when a different science goal is pursued. For practical purposes, however, it is useful to refer to a set of "default" cluster assignments, which we introduce here.

Initially, the coordinates of cluster centers are established by inspection of DSS images, with X-ray contours (from pointed *ROSAT* observations or the RASS data) overlaid. The type of center is recorded for future reference. Where there is clearly a dominant (usually cD) galaxy coincident with the X-ray peak, the center is denoted DX. If the center is defined by a pair or group of galaxies coincident with the X-ray peak, the code is GX. Centers derived from dominant galaxies offset from the X-ray peak are recorded as DG. Centers obtained from X-ray peaks with no obviously associated dominant galaxy are XP. In a few cases with complex X-ray substructure, the large-scale centroid of the X-ray emission is judged by eye, and the resulting cluster center is recorded with code XC.

The centers thus defined are used to define cluster "seeds" to which galaxies are to be assigned. The initial redshifts of the seeds are judged from the redshift histogram of galaxies in the field. Multiple cluster seeds are imposed if there are clearly several peaks in the velocity distribution (e.g., A1736AB, 0160AB, 1831AB, 1631AC, and A3526AB) or well-separated X-ray peaks (A0548AB, 2572AB, 3528AB, 1983AB, and 2572AB).

The assignments of galaxies to clusters are generated iteratively by comparing each galaxy to the redshift-space locations

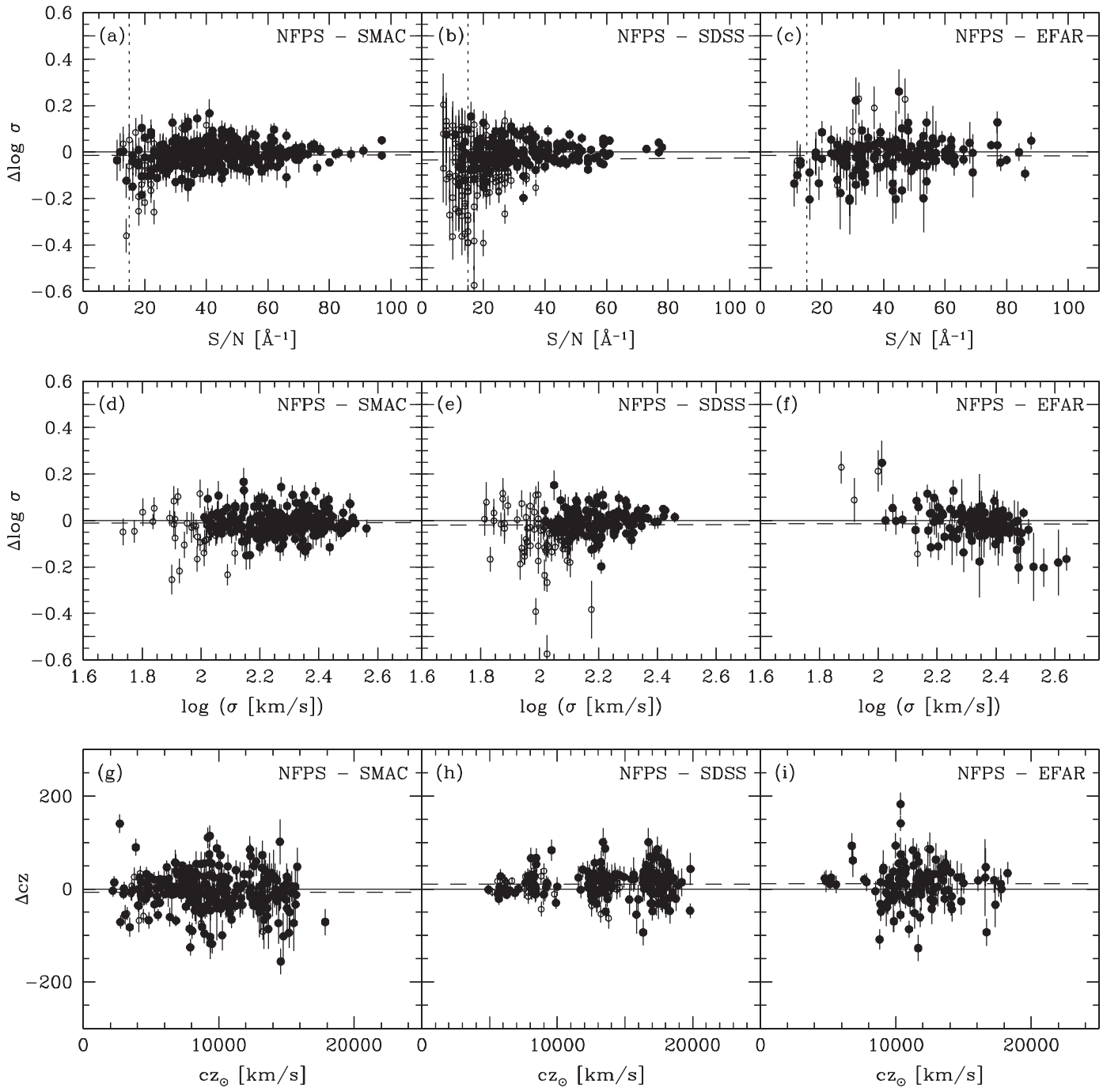

FIG. 6.—External comparisons of NFPS velocity dispersion and redshift measurements with those from the SMAC and EFAR catalogs (Hudson et al. 2001; Wegner et al. 1999) and the SDSS DR2 (Abazajian et al. 2004). (*a*)–(*c*): Differences in $\log \sigma$ (NFPS− external) plotted for each individual NFPS measurement, as a function of the NFPS S/N. The vertical dotted line indicates the limit at S/N = 15 Å^{-1}, below which the data do not contribute to the final merged catalog. (*d*)–(*f*): Comparison of merged velocity dispersion data plotted against the external (SMAC, SDSS, or EFAR) $\log \sigma$. (*g*)–(*i*): Equivalent comparisons for redshift differences Δcz (NFPS−external). Objects with $\sigma < 100$ km s^{-1} in either NFPS or the external study are denoted by open symbols. The dashed line gives the median offset in each comparison.

TABLE 4
EXTERNAL COMPARISONS OF $\log \sigma$

Comparison	$N_{\Delta \log \sigma}$	Mean Offset	Median	Scatter[a]
NFPS−SMAC.....	286	-0.012 ± 0.003	−0.009	0.046
NFPS−SDSS	203	-0.026 ± 0.006	−0.016	0.062
NFPS−EFAR.....	124	-0.013 ± 0.007	−0.015	0.052

[a] Nonparametric scatter; see text.

of cluster centers. To be assigned to a cluster, a galaxy must have a recession velocity cz within $\pm 3.5\sigma_{\rm cl}$ from the mean cluster redshift $cz_{\rm cl}$, where $\sigma_{\rm cl}$ is the radial velocity dispersion for the cluster. The galaxy must also lie within a projected radius $R < R_{\rm cl}$ of a cluster, where the cluster "radius" is defined by $R_{\rm cl} = 3(\sigma_{\rm cl}/1000 \text{ km s}^{-1})\, h^{-1}$ Mpc.

The cluster redshifts, $cz_{\rm cl}$, are updated after every iteration based on the new galaxy assignments. The dispersions, $\sigma_{\rm cl}$, are updated if a minimum of 10 member galaxies are available

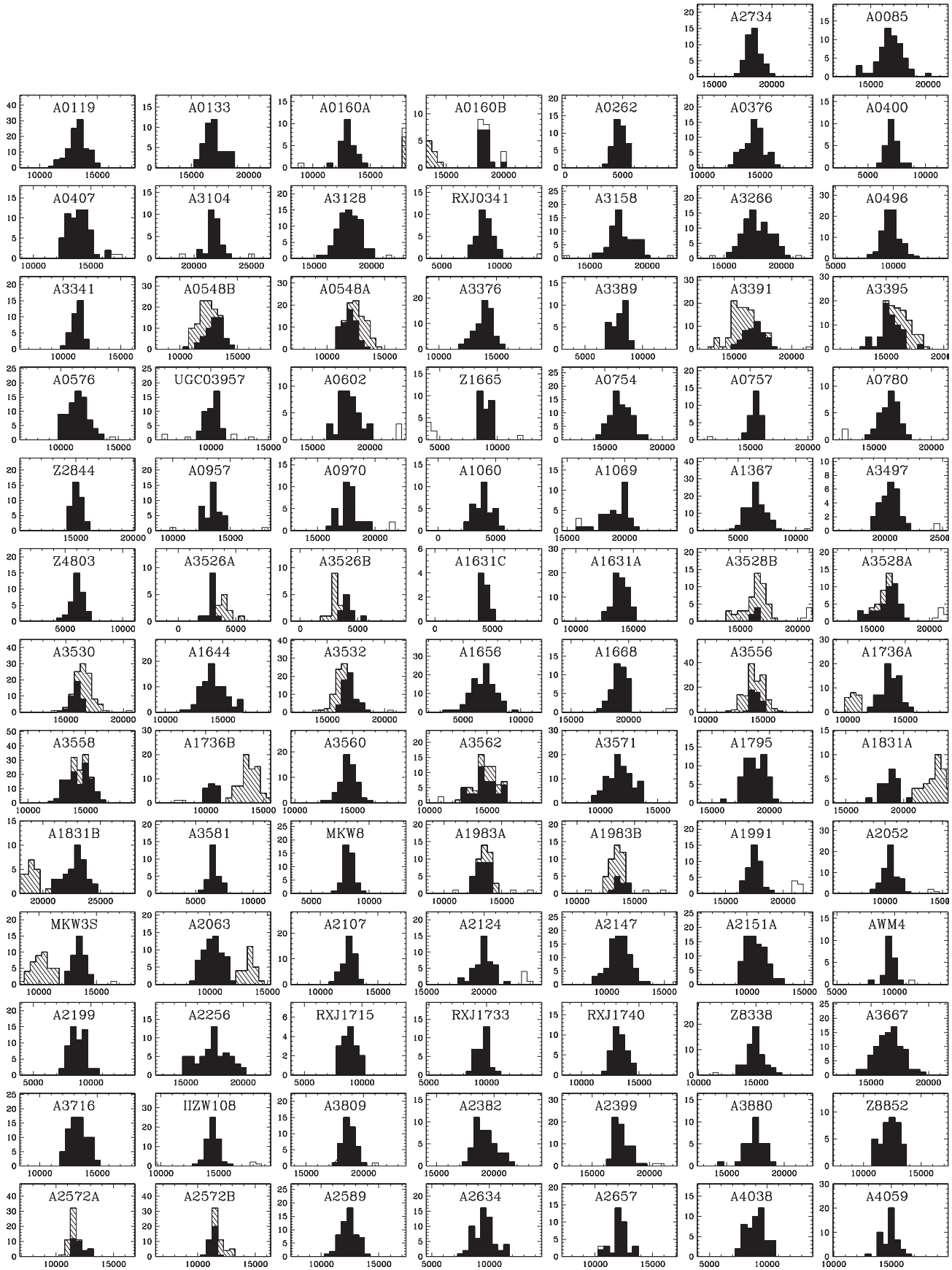

FIG. 7.—Redshift histograms of clusters in the NFPS sample. In each panel, the filled histogram shows the distribution of heliocentric velocities (in kilometers per second) for the galaxies assigned to the cluster. The light shaded region represents galaxies within 1° projected separation assigned to other clusters, whereas the unfilled portion shows galaxies assigned to none of the NFPS target clusters.

TABLE 5
MERGED SPECTROSCOPIC DATA FOR NFPS GALAXIES

Galaxy ID	R.A.[a] (J2000)	Decl.[a] (J2000)	N_{cz}[b]	$cz_{\odot}$[b]	ε_{cz}[b]	$(S/N)_{cz}$[b]	N_{σ}[c]	log σ[c]	$\varepsilon_{\log\sigma}$[c]	$(S/N)_{\sigma}$[c]	Cluster[d]
NFPJ001006.3−284623.....	2.52630	−28.77294	1	18,990	21	18	1	1.8772	0.0500	18	A2734
NFPJ001010.7−285020.....	2.54460	−28.83883	1	18,627	24	23	1	2.0410	0.0391	23	A2734
NFPJ001014.2−290502.....	2.55915	−29.08397	1	37,447	38	10	...	...	...	...	...
NFPJ001024.3−284935.....	2.60145	−28.82636	1	17,924	31	22	1	2.2337	0.0409	22	A2734
NFPJ001032.5−285154.....	2.63520	−28.86503	1	17,442	32	19	1	2.1562	0.0474	19	A2734

NOTE.—Table 5 is presented in its entirety in the electronic edition of the Astronomical Journal. A portion is shown here for guidance regarding its form and content.

[a] Galaxy coordinates are given in degrees of R.A. and decl. and are expected to be accurate to $\lesssim 1''$.

[b] The heliocentric redshift $cz_{\odot}$ is quoted in kilometers per second, with error ε_{cz}. The value derives from merging N_{cz} individual measurements with effective total signal-to-noise ratio $(S/N)_{cz}$ per angstrom.

[c] The logarithm of the velocity dispersion σ (in kilometers per second), with error $\varepsilon_{\log\sigma}$. The value derives from merging N_{σ} individual measurements with effective total signal-to-noise ratio $(S/N)_{\sigma}$ per angstrom. Only spectra with $S/N > 15$ are allowed to contribute to the merged data, so in some cases $(S/N)_{\sigma} > (S/N)_{cz}$. The $\log\sigma$ values are as observed through a $2''$ diameter fiber; no aperture corrections have been applied.

[d] The cluster to which the galaxy is assigned by the algorithm discussed in the text. Missing data in this column indicate either that no redshift measurement was achieved or that the galaxy is not assigned to any cluster. Stars are indicated by the entry "star."

for the calculation and subject to a stabilizing condition that 500 km $s^{-1} \leq \sigma_{cl} \leq 1000$ km s^{-1}. Note that while literature values for σ_{cl} may in some cases be a more accurate reflection of the dispersion for all galaxies, for consistency of assignments across the NFPS sample, we require the velocity dispersions of only the red galaxies. For robustness against outliers, an estimator based on interpercentile range is used to calculate σ_{cl}. The projected centers of the clusters are not updated as the assignment proceeds, since these have been defined more robustly by external criteria (cD galaxies and X-ray peaks).

Occasionally, a galaxy satisfies the assignment criteria for more than one cluster. In these cases, the galaxy is assigned to the cluster that minimizes the statistic

$$C = (cz - cz_{cl})^2/\sigma_{cl}^2 - 4\log(1 - R/R_{cl}).$$

This quantity is proportional to the logarithm of the probability that a given galaxy is a member of a given cluster under a simple model. The velocity probability assumes that the cluster velocity distribution is a Gaussian. For the radial probability, one might have assumed that the number density of galaxies is $\propto r^{-2}$ in three dimensions and hence $\propto R^{-1}$ in two-dimensional projection. This scheme, however, would give diverging weight to objects near cluster centers, the positions of which are not precisely known. A simple linear scheme, $p(R) \propto (1 - R/R_{cl})$, is more robust both to errors in the cluster center and to errors in R_{cl}. The weighting factor of 4 (which trades between velocity weight and position weight) was chosen to give the best match between assignments by the objective algorithm and those made "by eye" for several close cluster pairs. In Figure 7, we show the redshift distribution of NFPS galaxies in each of the 93 clusters observed.

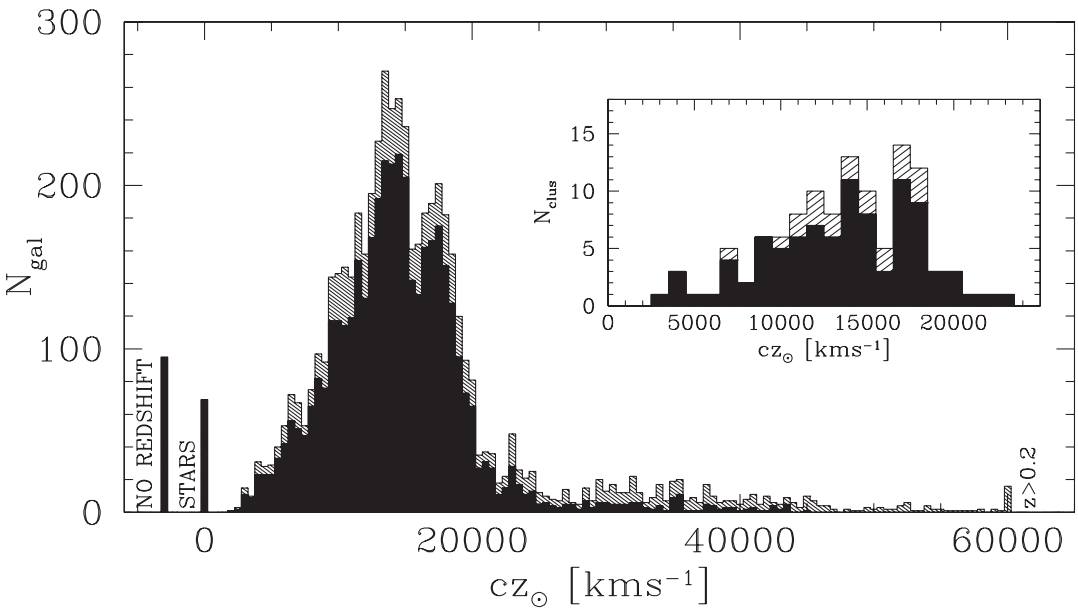

FIG. 8.—Redshift histograms of the NFPS spectroscopic sample. In the main panel, the dark portion shows galaxies with velocity dispersion measurements, while the lighter region indicates additional objects lacking dispersion data. The last bin includes all objects with $cz > 60{,}000$ km s^{-1}. The two bars at the left arise from misidentified stars (at $cz \sim 0$) and observed objects that yielded no redshift measurement (arbitrarily placed at $cz = -3000$ km s^{-1}. The inset panel shows the histogram of mean velocities for NFPS clusters; clusters without spectroscopic follow-up data are shown with lighter shading. Note that the strong peaks at ~14,000 and ~17,000 km s^{-1} are reproduced in both the galaxy and cluster distributions.

4. DATA SUMMARY

The final merged data set is presented in Table 5, which lists all 5479 observed galaxies. Of these, 5388 (98%) have redshift measurements, while the velocity dispersion has been measured for 4131 (75%). The median estimated velocity dispersion error is 7%. The redshift distribution of the whole spectroscopic sample is presented in Figure 8.

Future papers in this series will present emission- and absorption-line–strength indices (Nelan et al. 2004) and the photometric and morphological parameters. Combined with the spectroscopic measurements presented here, these data will subsequently be applied to the twin goals of NFPS: the study of the peculiar velocity field on the largest scales and the investigation of the formation history of galaxies in the cluster environment.

We gratefully acknowledge the substantial assignment of NOAO observing resources to the NFPS program. We wish especially to thank Knut Olsen and Riccardo Venegas at Cerro Tololo and Diane Harmer at WIYN for their expert support of the Hydra observations. R. J. S. was supported for part of this research by the Chilean CONICYT through Proyecto FONDECYT 3990025. M. J. H. acknowledges support from the NSERC of Canada, an Ontario Premier's Research Excellence Award, and a Chretien International Research Grant from the American Astronomical Society. S. A. W. M. was supported from the PPARC grant "Extragalactic Astronomy & Cosmology at Durham 1998–2002." S. J. Q. was supported by a PPARC studentship. IRAF is distributed by the National Optical Astronomy Observatory, which is operated by the Association of Universities for Research in Astronomy, Inc. under contract with the National Science Foundation. This research has made use of the NASA/IPAC Extragalactic Database (NED), which is operated by the Jet Propulsion Laboratory, California Institute of Technology, under contract with the National Aeronautics and Space Administration.

REFERENCES

Aaronson, M., Bothun, G., Mould, J., Huchra, J., Schommer, R. A., & Cornell, M. E. 1986, ApJ, 302, 536
Abazajian, K., et al. 2004, AJ, 128, 502
Abell, G. O. 1958, ApJS, 3, 211
Abell, G. O., Corwin, H. G., Jr., & Olowin, R. P. 1989, ApJS, 70, 1
Batuski, D. J., Bahcall, N. A., Olowin, R. P., & Burns, J. O. 1989, ApJ, 341, 599
Bernardi, M., et al. 2003, AJ, 125, 1817
Bertin, E., & Arnouts, S. 1996, A&AS, 117, 393
Colless, M., Saglia, R. P., Burstein, D., Davies, R. L., McMahan, R. K., & Wegner, G. 2001, MNRAS, 321, 277
Collins, C. A., Guzzo, L., Nichol, R. C., & Lumsden, S. L. 1995, MNRAS, 274, 1071
Dale, D. A., Giovanelli, R., Haynes, M. P., Campusano, L. E., Hardy, E., & Borgani, S. 1999, ApJ, 510, L11
de Grandi, S., et al. 1999, ApJ, 514, 148
Dekel, A. 1994, ARA&A, 32, 371
Dressler, A. 1980, ApJS, 42, 565
Dressler, A., Lynden-Bell, D., Burstein, D., Davies, R. L., Faber, S. M., Terlevich, R., & Wegner, G. 1987, ApJ, 313, 42
Ebeling, H., Edge, A. C., Böhringer, H., Allen, S. W., Crawford, C. S., Fabian, A. C., Voges, W., & Huchra, J. P. 1998, MNRAS, 301, 881
Ebeling, H., Voges, W., Böhringer, H., Edge, A. C., Huchra, J. P., & Briel, U. G. 1996, MNRAS, 281, 799
Hogg, D. W., & Turner, E. L. 1998, PASP, 110, 727
Hudson, M. J. 2004, in Proc. 15th Rencontres De Blois, Physical Cosmology: New Results In Cosmology and the Coherence of the Standard Model, ed. J. Bartlett, in press
Hudson, M. J., Lucey, J. R., Smith, R. J., Schlegel, D. J., & Davies, R. L. 2001, MNRAS, 327, 265
Hudson, M. J., Smith, R. J., Lucey, J. R., & Branchini, E. 2004, MNRAS, 352, 61
Hudson, M. J., Smith, R. J., Lucey, J. R., Schlegel, D. J., & Davies, R. L. 1999, ApJ, 512, L79
Jørgensen, I., Franx, M., & Kjærgaard, P. 1995, MNRAS, 276, 1341
Kinney, A. L., Calzetti, D., Bohlin, R. C., McQuade, K., Storchi-Bergmann, T., & Schmitt, H. R. 1996, ApJ, 467, 38
Landolt, A. U. 1992, AJ, 104, 340
Lauer, T. R., & Postman, M. 1994, ApJ, 425, 418
Lucey, J. R., Guzmán, R., Steel, J., & Carter, D. 1997, MNRAS, 287, 899
Lynden-Bell, D., Faber, S. M., Burstein, D., Davies, R. L., Dressler, A., Terlevich, R. J., & Wegner, G. 1988, ApJ, 326, 19
Monet, D., et al. 1998, The USNO-A2.0 Catalogue (Flagstaff: USNO)
Nelan, J. E., et al. 2004, in preparation
Reiprich, T. H., & Böhringer, H. 2002, ApJ, 567, 716
Smith, R. J., Lucey, J. R., Hudson, M. J., Schlegel, D. J., & Davies, R. L. 2000, MNRAS, 313, 469
Smith, R. J., Lucey, J. R., Steel, J., & Hudson, M. J. 1997, MNRAS, 291, 461
Stetson, P. B. 2000, PASP, 112, 925
Strauss, M. A., & Willick, J. A. 1995, Phys. Rep., 261, 271
Teague, P. F., Carter, D., & Gray, P. M. 1990, ApJS, 72, 715
Tonry, J. L., & Davis, M. 1981, ApJ, 246, 666
Voges, W. 1992, in Environment Observation and Climate Modelling Through International Space Projects, ed. T. D. Guyenne & J. J. Hunt (ESA ISY-3; Noordwijk: ESA), 9
Wegner, G., et al. 2003, AJ, 126, 2268
Wegner, G., Colless, M., Saglia, R. P., McMahan, R. K., Jr., Davies, R. L., Burstein, D., & Baggley, G. 1999, MNRAS, 305, 259
Willick, J. A. 1999, ApJ, 522, 647